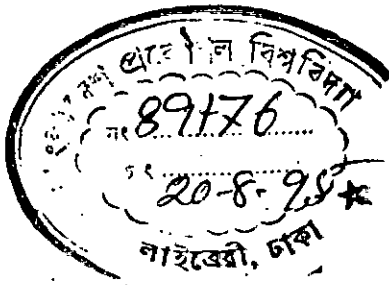


A STUDY OF INVERSION LAYER QUANTUM CAPACITANCE OF MOS STRUCTURES

A Thesis submitted to the Electrical and Electronic
Engineering Department of BUET, Dhaka,
in partial fulfilment of the
requirements for the degree of
Master of Science in Engineering
(Electrical and Electronic)



MAHERIN MATIN

AUGUST 1995



#89176#

The thesis 'A study of inversion layer quantum capacitance of MOS structures' submitted by Maherin Matin, Roll No.921356F, session 1990-91-92 to the Electrical and Electronic Engineering Department of BUET has been accepted as satisfactory for partial fulfilment of the requirements for the degree of Master of Science in Engineering (Electrical and Electronic).

Board of Examiners

1. Dr. M.M. Shahidul Hassan
Associate Professor
EEE Department
BUET., Dhaka-1000

Chairman
(Supervisor)

M. M. Shahidul Hassan
8/8/95

2. Dr. A.B.M. Siddique Hossain
Professor & Head
EEE Department
BUET., Dhaka-1000

Member
(Ex-officio)

A. B. M. Siddique Hossain
03/08/95

3. Dr. Saiful Islam
Professor & Dean
EEE Faculty
BUET., Dhaka-1000

Member

Saiful Islam
3/8/95

4. Dr. M. Ali Asgar
Professor & Dean
Faculty of Engineering
BUET., Dhaka-1000

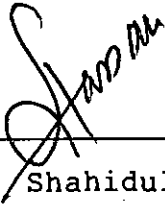
Member
(External)

M. A. Asgar
3/8/95

DECLARATION

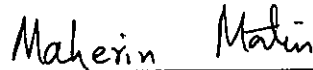
I hereby declare that this work has been done by me and it has not been submitted elsewhere for the award of any degree or diploma.

Countersigned



(Dr. M.M. Shahidul Hassan)

Supervisor



(Maherin Matin)

CONTENTS

ACKNOWLEDGEMENTS	iv
ABSTRACT	v
LIST OF FIGURES	vi
1. INTRODUCTION	1
1.1 Capacitance of a MOS structure.....	1
1.2 Quantum effects on inversion layer capacitance...	11
1.3 Review of recent works on MOSFET capacitance.....	14
1.4 Objective of this work.....	15
1.5 Summary of the thesis.....	16
2. MATHEMATICAL ANALYSIS FOR CAPACITANCE OF MOS STRUCTURES CONSIDERING QUANTUM EFFECTS	17
2.1 Introduction.....	17
2.2 Sub-bands of a triangular potential well.....	19
2.2.1 Airy function approximation.....	19

2.2.2	Triangular potential approximation.....	19
2.2.3	Approximate solution.....	20
2.3	Population of carriers in the two sub-bands.....	29
2.4	Average separation of minority carriers from the interface.....	30
2.5	An analytical expression for inversion layer quantum capacitance.....	31
2.6	Summary.....	40
3.	RESULTS BASED ON ANALYTICAL SOLUTION	41
3.1	Introduction.....	41
3.2	Computational method in studying MOS device.....	41
3.3	Results and discussions.....	42
3.3.1	Quantization of energy levels.....	42
3.3.2	Inversion layer charge concentration.....	45
3.3.3	Depletion layer charge concentration.....	45
3.3.4	Electron concentrations in the two sub-bands.....	45
3.3.5	Average spatial extent of the inversion layer electrons from the surface.....	49
3.3.6	Inversion layer capacitance.....	49
3.4	Summary.....	53

4. CONCLUSIONS 55

4.1 Conclusions..... 55

4.2 Suggestions for future work..... 56

REFERENCES 57

ACKNOWLEDGEMENTS

The author would like to express her deep gratitude and appreciation to Dr. M.M. Shahidul Hassan, Associate Professor of the Department of Electrical and Electronic Engineering, BUET, for his continued guidance, enthusiasm, encouragement and valuable suggestions while performing this work.

The author wishes to express her thanks and regards to Dr. A.B.M. Siddique Hossain, Professor and Head of the Department of Electrical and Electronic Engineering, BUET, for his support to complete this work.

The author is indebted to her parents and husband for their endless support. Thanks to all friends and colleagues for their cooperation.

ABSTRACT

MOSFETs are extensively used in IC fabrication. Improvement of the VLSI technology has resulted in device dimensions of the order of fractions of a micron. In MOSFETs with increased substrate doping levels and reduced gate oxide thicknesses the energy-band bending at the Si/SiO₂ interface, under inversion condition, is very steep. Quantum effects arise when the confinement of inversion layer carriers in this potential well yields an increasingly two-dimensional carrier system and the classical treatment of MOSFETs is no longer accurate. The effects of quantization can be most accurately modeled by solving the Schrödinger's and Poisson's equations self-consistently. The quantum mechanical calculation is very time consuming and therefore, it is necessary to develop a simple model which includes the quantization effects and requires less computational time.

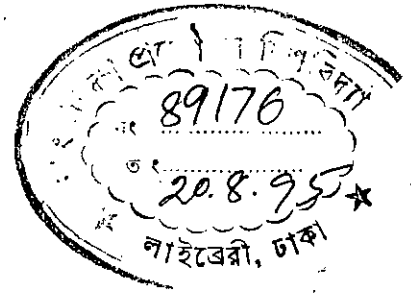
In this thesis the eigen energies of the potential well are determined by solving Schrödinger's wave equation for a triangular potential well by Airy function approximations. To find an analytical expression for quantum capacitance, the electron population in two sub-bands are considered. The capacitance calculated considering quantum effects is found to deviate from the classical value.

LIST OF FIGURES

1.1	The metal oxide-semiconductor capacitor.....	2
1.2	Substrate energy band diagram.....	5
1.3	Substrate band diagram at higher gate voltage.....	7
1.4	Electron concentration at the surface vs. surface potential.....	8
1.5	Quantum-mechanical effects on inversion layer charge.....	13
2.1	Energy sub-bands in a triangular potential well.....	21
2.2	Charge distribution in a MOS structure.....	34
2.3	Band bending due to depletion charges.....	35
3.1	Effect of surface electric field on the energy levels.....	43
3.2	Energy levels vs. inversion layer charge.....	44
3.3	Effect of surface potential on the inversion layer charge.....	46
3.4	Effect of surface potential on depletion layer charge.....	47
3.5	Electron concentration of the two sub-bands vs. surface potential.....	48
3.6	Average separation of carriers vs. inversion layer charge.....	50
3.7	Average separation of carriers vs. surface potential.....	51
3.8	Effect of surface potential on the classical and quantum mechanical capacitances.....	52

CHAPTER 1

INTRODUCTION



1.1 Capacitance of a MOS-structure

The metal-oxide - semiconductor (MOS) structure is, without a doubt, the core structure in modern day microelectronics. With dc current flow blocked by the oxide, the major observable exhibited by a MOS-structure is capacitance. As it turns out the capacitance varies as a function of the applied gate voltage and the capacitance-voltage (C-V) characteristic is of considerable practical importance. The C-V characteristics are routinely monitored during MOS device fabrication.

As pictured in (Fig.1.1) the MOS-capacitor is a simple two-terminal device composed of a thin (0.01 μm -1.0 μm) SiO_2 layer sandwiched between a silicon substrate and a metallic field plate called gate. The most common field plate materials are aluminium and heavily doped polycrystalline silicon. A second metallic plate which provides an electrical contact to the silicon substrate,

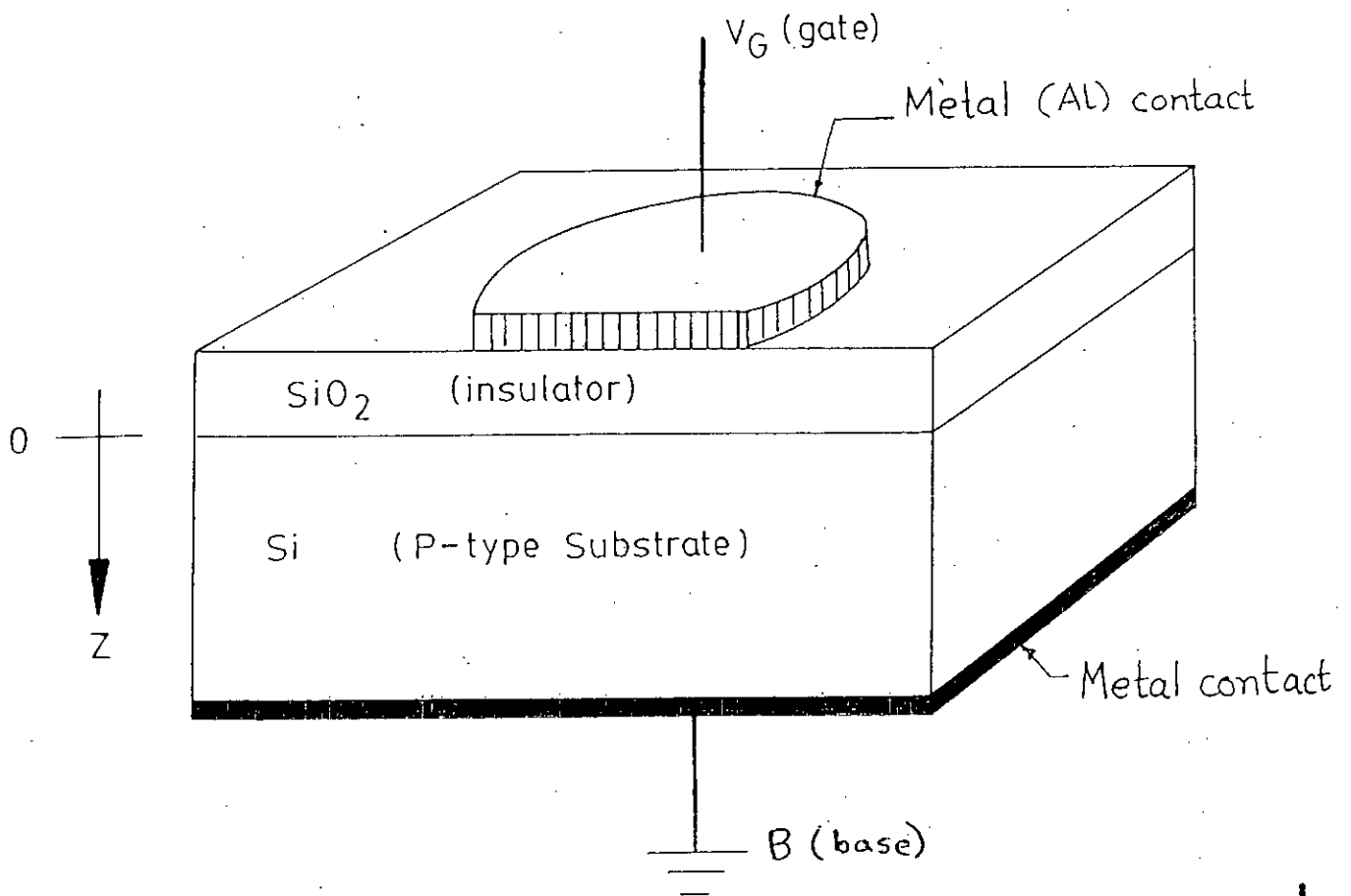


Fig. 1.1 The metal oxide-semiconductor capacitor.

which is normally grounded, is called the substrate contact.

The ideal MOS structure has the following explicit properties:

- (i) The metallic gate is sufficiently thick so that it can be considered an equipotential region biasing conditions;
- (ii) The oxide is a perfect insulator with zero current flowing through the oxide layer under all static biasing conditions;
- (iii) There are no charge centers located in the oxide or at the oxide semiconductor interface;
- (iv) The semiconductor is uniformly doped;
- (v) The semiconductor is sufficiently thick so that, regardless of the applied gate potential; a field-free region (the so called "bulk") is encountered before reaching the back contact.

Electron and hole concentrations in the p-type substrate are given [1] as:

$$n = n_i e^{(\psi - \phi_p) \frac{q}{kT}} \quad (1.1)$$

and

$$p = n_i e^{(\phi_p - \psi) \frac{q}{kT}} \quad (1.2)$$

where, n_i is the intrinsic carrier concentration, K is the Boltzmann's constant, T is the absolute temperature, ψ and ϕ_f are the potentials of the intrinsic energy level and Fermi level respectively (Fig.1.2).

The electric field ($\xi = -\frac{d\psi}{dz}$) is assumed to vanish as one proceeds into the semiconductor substrate. Following standard convention, the intrinsic level potential ψ is chosen to be zero in the field-free region of the substrate referred to as the semiconductor bulk. ψ evaluated at the oxide-semiconductor interface (at $z=0$) is given the special symbol ψ_s and is known as the surface potential (Fig.1.2).

Taking the intrinsic level potential in the bulk region of the substrate as zero, the electron concentration can be written as,

$$n = N_A e^{(\psi - 2\phi_f) \frac{q}{kT}} \quad (1.3)$$

where, N_A is the doping density of the p-type substrate.

Positive gate voltage produces an electric field which bends the energy bands downward. For a small positive gate voltage (V_G) the majority carriers (holes) are depleted from the vicinity of the

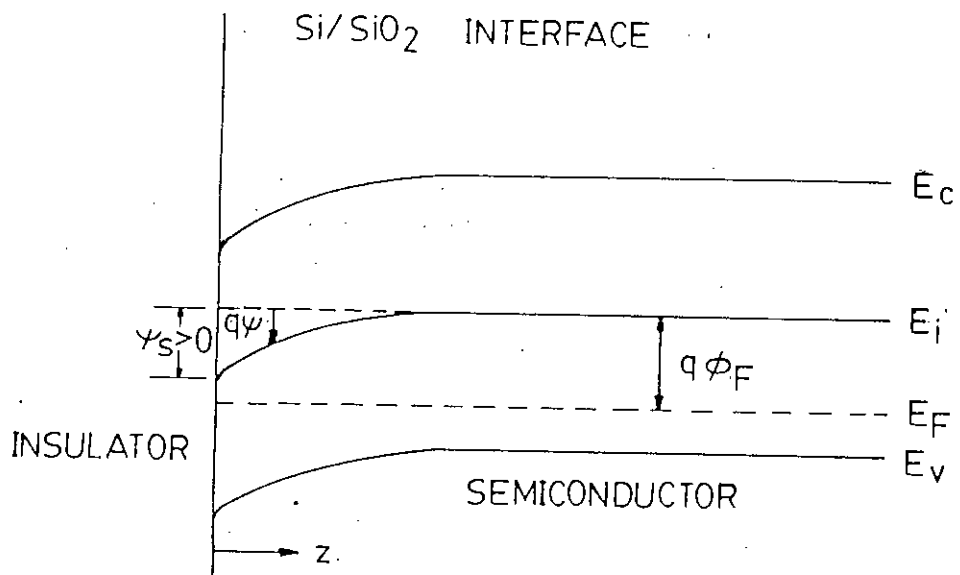


Fig. 1.2 Substrate energy band diagram.

oxide-silicon surface, establishing a space charge region consisting of stationary acceptor ions (Fig.1.3a). As V_G is increased further, more acceptor atoms are uncovered and ψ_s becomes sufficiently positive to attract a significant number of free electrons to the surface. We consider that these electrons come from the relatively slow process of electron hole generation in the depletion region, caused by the thermal vibration of the lattice. Eventually, a sufficiently high V_G can bend E_i below E_F and the density of electron will exceed that of holes at the surface and we have surface inversion. This situation is illustrated in (Fig.1.3b).

The electron concentration at the surface is given by:

$$n_{\text{surface}} = N_A e^{(\psi_s - 2\phi_F) \frac{q}{kT}} \quad (1.4)$$

At $\psi = \phi_F$, $n_{\text{surface}} = n_i$; intrinsic concentration as seen from equation (1.1) and from $np = n_i^2$ then, $n_{\text{surface}} = p_{\text{surface}} = n_i$ this is defined as the limit point between the depletion and inversion regions. With increasing ψ_s above ϕ_F , n_{surface} increases drastically, and at $\psi_s = 2\phi_F$ we have $n_{\text{surface}} = N_A$ and this situation is shown in (Fig.1.4).

The density of the induced charge below the oxide denoted by Q_s , is given by Gauss' law

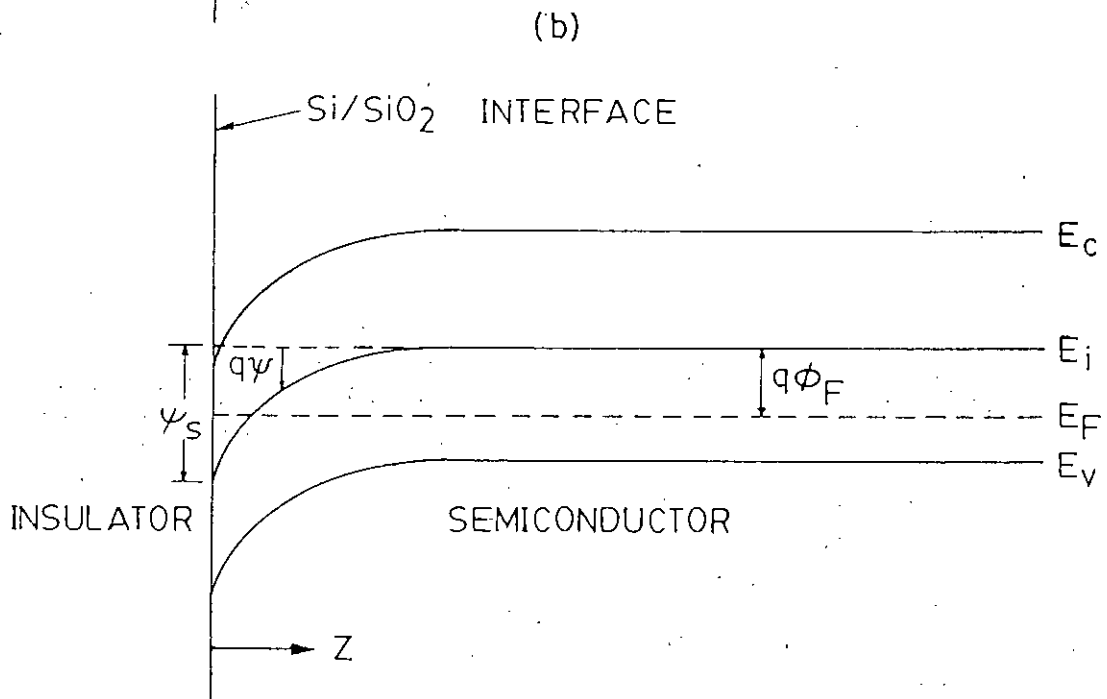
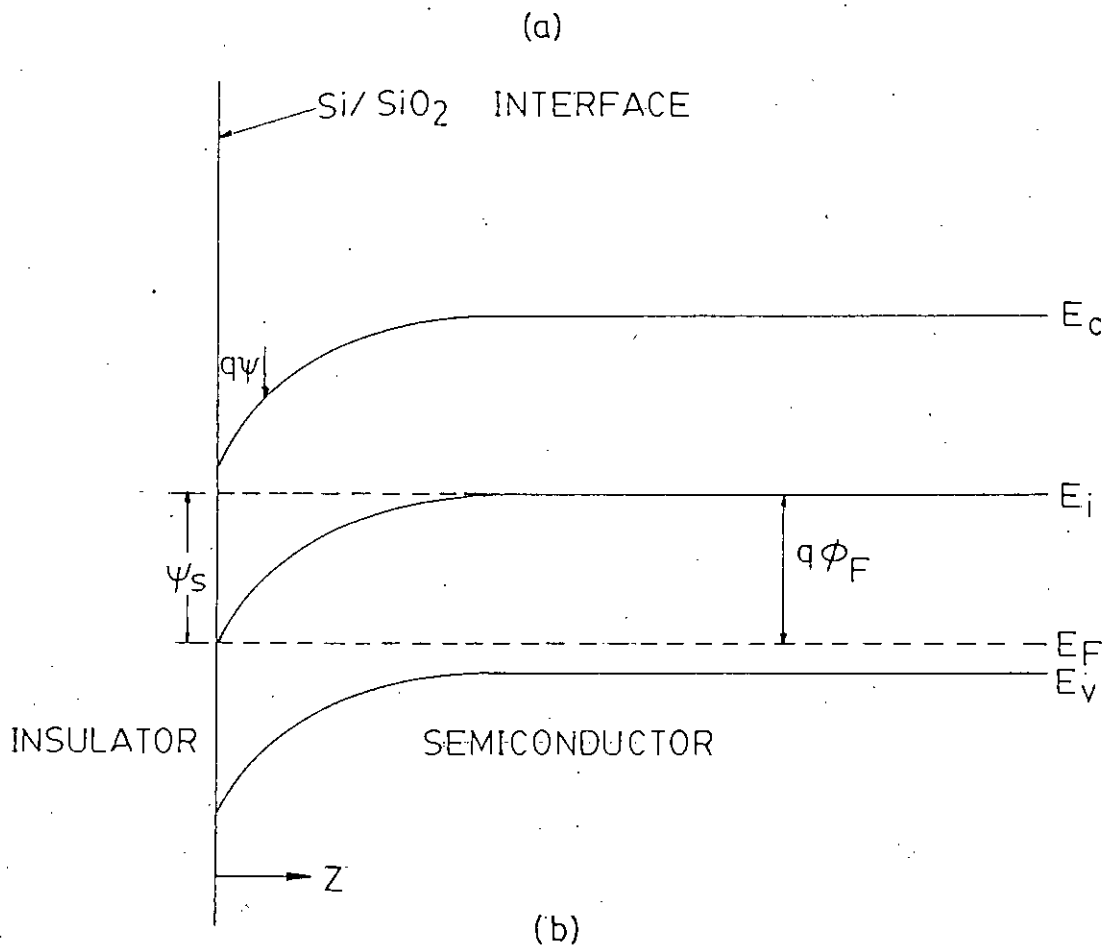


Fig. 13 Substrate band diagram at higher gate voltage.
 (a) depletion (b) inversion.

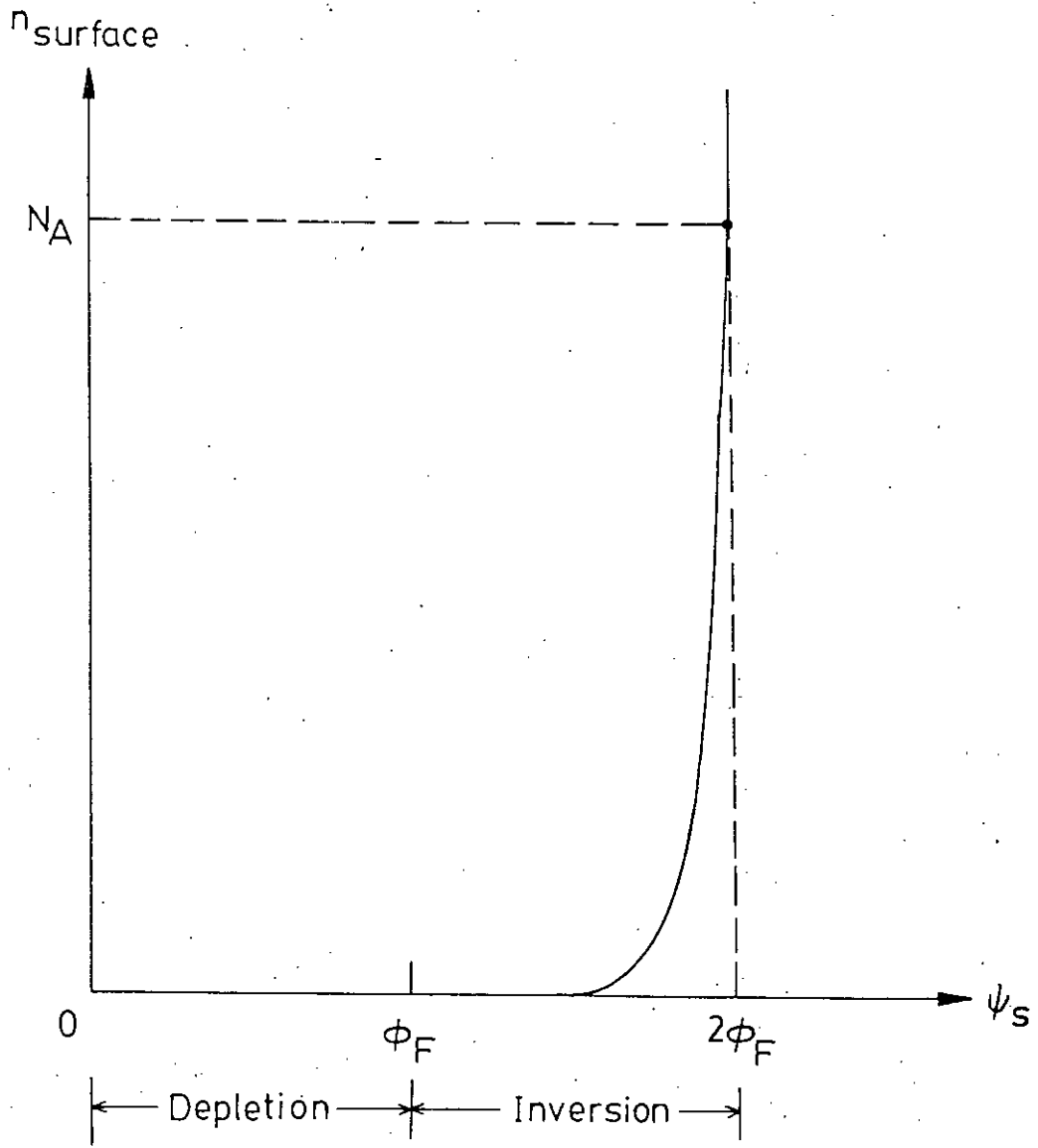


Fig. 1.4 Electron concentration at the surface vs. surface potential.

$$-Q_s = k_{ox} \epsilon_0 F_{ox} = k_s \epsilon_0 F_s \quad (1.5)$$

where ϵ_0 = free-space permittivity

k_{ox} = dielectric constant of oxide

F_{ox} = electric field in the oxide.

k_s = dielectric constant of semiconductor.

F_s = field at the semiconductor surface.

The electric field at the interface is given by [2],

$$F_s = \pm \frac{F\sqrt{N_A}}{\epsilon_s} \sqrt{(\phi_t e^{-\frac{\psi_s}{\phi_t}} + \psi_s - \phi_t) + e^{-\frac{2\phi_f}{\phi_t}} (\phi_t e^{\frac{\psi_s}{\phi_t}} - \psi_s - \phi_t)} \quad (1.6)$$

where $F = \sqrt{2q\epsilon_s}$ and the + sign for F_s is to be used with ψ_s

> 0 , and the - sign with $\psi_s < 0$; $\phi_t = kT/q$, and the total semiconductor charge per unit area Q_s , is given as :

$$Q_s = \mp F\sqrt{N_A} \sqrt{(\phi_t e^{-\frac{\psi_s}{\phi_t}} + \psi_s - \phi_t) + e^{-\frac{2\phi_f}{\phi_t}} (\phi_t e^{\frac{\psi_s}{\phi_t}} - \psi_s - \phi_t)} \quad (1.7)$$

The total charge (per unit area) below the oxide is the sum of the charge due to the electrons in the inversion layer Q_I and the charge due to the ionized acceptor atoms in the depletion region Q_B

$$Q_s = Q_I + Q_B \quad (1.8)$$

The small-signal capacitance per unit area corresponding to the semiconductor charge region is denoted by,

$$C_s = - \frac{dQ_s}{d\psi_s} \quad (1.9)$$

from equation (1.8),

$$C_s = \frac{-dQ_I}{d\psi_s} + \frac{-dQ_B}{d\psi_s} \quad (1.10)$$

We have then separated the total semiconductor capacitance C_s into two components, one owing to the depletion region charge and one owing to the inversion layer charge. So we can define an inversion region incremental capacitance per unit area ,

$$C_I = \frac{-dQ_I}{d\psi_s} \quad (1.11)$$

This capacitance relates changes in the charge of the inversion

layer to the associated potential changes.

We can also define a depletion region incremental capacitance per unit area:

$$C_b = \frac{-dQ_B}{d\psi_s} \quad (1.12)$$

This capacitance relates changes of the potential across the depletion region to the associated changes of the charge in it. The resulting exact C_i and C_b are given by [2]

$$C_i = F\sqrt{N_A} \frac{e^{\frac{(\psi_s - 2\phi_p)}{\phi_c}}}{2\sqrt{\psi_s + \phi_c} e^{\frac{(\psi_s - 2\phi_p)}{\phi_c}}} \quad (1.13)$$

$$C_b = F\sqrt{N_A} \frac{1}{2\sqrt{\psi_s + \phi_c} e^{\frac{(\psi_s - 2\phi_p)}{\phi_c}}} \quad (1.14)$$

1.2 Quantum effects on inversion layer capacitance.

The interest in MOS structure is enhanced because they show the

electronic properties expected of a 2-DEG electron gas. Quantum effects arise when band bending confines the carriers to a narrow surface channel. The combination of thinner gate oxides and higher levels of channel doping increases the electric field associated with inversion layer to such an extent that it produces a potential well whose width, in the z-direction, the direction perpendicular to the surface, is small compared to the wavelength of the carriers. It is clear that if the carrier wavelength is comparable to the distance from the interface to the classical turning point ($\frac{E_1}{qF_s}$) then quantization of the motion in this direction into discrete levels is expected i.e. a 2-DEG gas is formed [3].

The Quantum mechanical picture differs in several aspects from the classical one [4]. First of all, the energy spectrum consists of a set of discrete energy levels and the first allowed energy level E_0 does not coincide with the bottom of the conduction band E_c (Fig.1.5). This energy difference increases as MOS devices are scaled down because the channel doping N_A increases. This effectively widens the band gap for all temperatures and hence a larger surface potential is needed for a given channel charge. The quantization of energy has the effect of decreasing the inversion layer charge density for a given gate voltage.

The second quantum mechanical effect to be taken into account is that the average distance of the spatial distribution of the

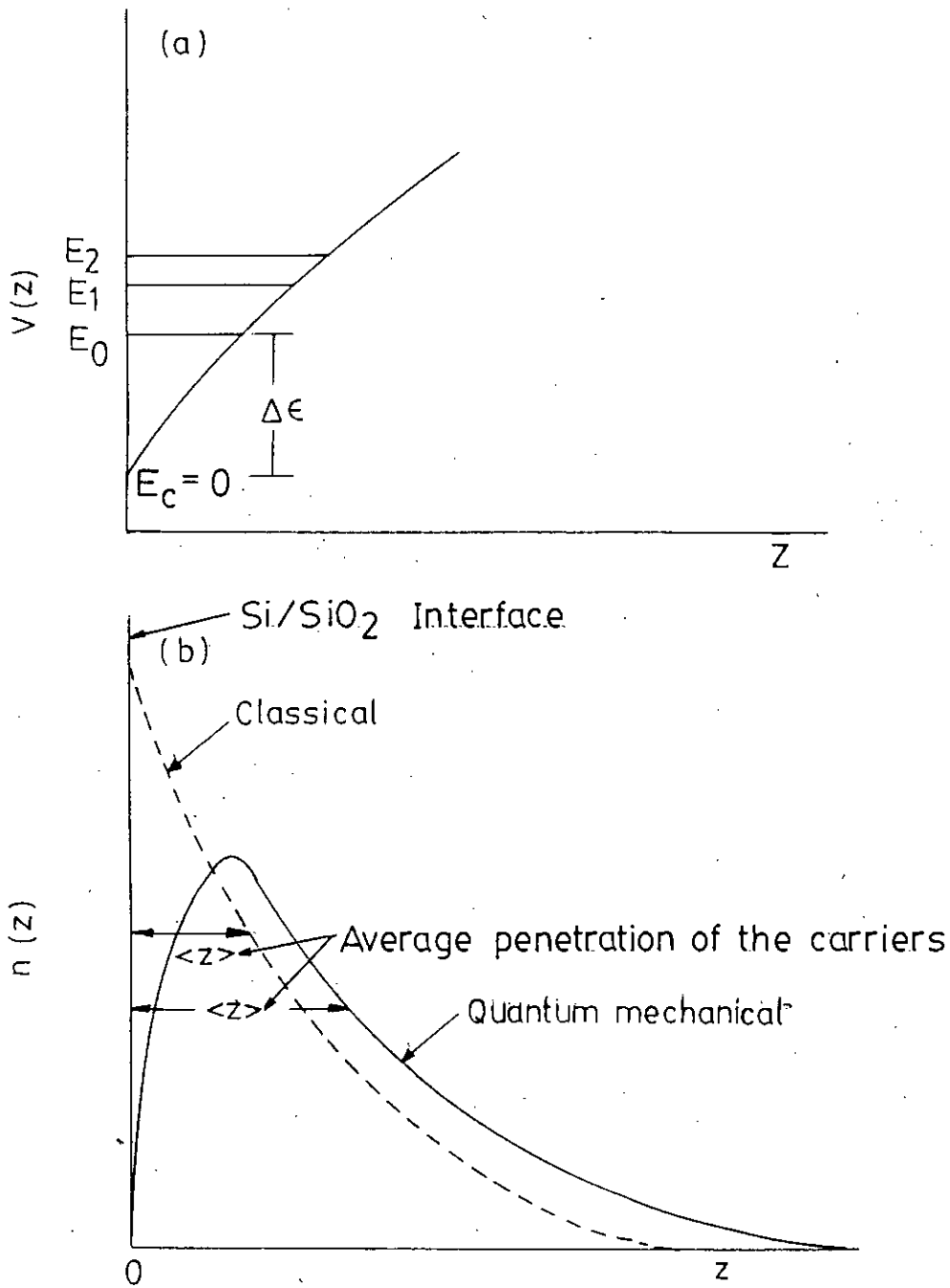


Fig. 1.5 Quantum mechanical effects on inversion layer charge.
 (a) Energy layer split.
 (b) Spatial distribution of carriers.

inversion layer charge from the interface is larger in the quantum-mechanical framework. Hence, a larger band bending is needed for a given population in the conduction band.

Considering all these effects we conclude that the inversion layer capacitance (C_{inv}) is decreased when compared with the classical value.

1.3 Review of recent works on MOSFET Capacitance.

The need for careful treatment of inversion layer quantization has recently become more pressing due to the increasing impact of the quantization on low dimension MOSFET characteristics with the reduced gate oxide thickness and increased channel doping required in scaled devices. The quantum nature of the two dimensional electron gas in MOSFETs has been studied in detail in Ref [3].

Two dimensional (2-DEG) electron gas in a quantum well or inversion layer, unlike an ordinary grounded metallic plate, does not completely screen an applied electric field. A 2-DEG manifests itself as a capacitor in series in the direction transverse to the quantum well [5]. Recent works on this issue were carried out mostly on double barrier structures [6] and a few numerical works have been done on MOS structures [7]. To find the expression of

capacitance of a double-barrier structure, the Fermi level was not considered horizontal. By taking the derivative of electron concentration in sub-bands with respect to the Fermi level an expression of capacitance was determined. In contrary to this, in MOS structures the SiO_2 acts as an insulator and prevents the current flow through it so that the Fermi level is flat. The derivative of carriers in the subbands with respect to the surface potential gives the expression for capacitance in this case.

1.4 Objective of this work

The effects of quantization on MOS device behavior have been known for decades. Recently it has become important and necessary to physically account for these effects in MOS device at room temperature. The main objective of this research is to establish an analytical expression of inversion layer capacitance considering quantization effects in the MOS-structures. In this thesis, expression for eigen energies of sub-bands is derived by applying Airy function approximation method for a triangular potential well in MOS under inversion. The electron population in the two consecutive sub-bands are then related with the two sub-band energies. Expression for surface potential is established as a function of total electron concentration N_{inv} in the inversion layer. Differentiating the total electron concentration with

respect to the surface potential the quantum capacitance expression is found out. This work also compares the inversion layer quantum capacitance with the classical one.

1.5 Summary of the thesis

In this thesis an analytical expression for inversion layer capacitance considering quantization effects in the MOS-structure is established. The Schrödinger's wave equation is solved using Airy function approximation in chapter 2. An analytical model to calculate inversion layer quantum capacitance is discussed and expression for capacitance is also established in chapter 2.

The results of the quantum mechanical effects on inversion layer charge concentration, the spatial distribution of carriers inside the potential well, the electron concentration in the lowest and the first energy sub-bands and also the predicted difference between classically and quantum mechanically calculated inversion layer capacitances are given in chapter 3. Chapter 4 contains the concluding remarks along with recommendations for future work on this topics.

CHAPTER 2

MATHEMATICAL ANALYSIS FOR CAPACITANCE OF MOS-STRUCTURES CONSIDERING QUANTUM EFFECTS

2.1 Introduction

It is well-known that the motion of the electrons perpendicular to the Si-SiO₂ interface of a MOS structure is quantized, because the electrons are confined to a well-defined potential well in this direction. In quantum mechanical picture the energy spectrum consists of a discrete set of energy levels. The lowest energy level is shifted substantially above the conduction band minimum.

The charge density, quantum mechanically, goes essentially to zero in the oxide because of the high barrier here and has its peak well inside the silicon. The classical Thomas-Fermi solution, in which the charge density depends only on the local separation of the band edge and the Fermi level, has a peak at the interface. In addition, the average spatial extent of the

charge from the interface is greater when calculated quantum mechanically than when calculated classically.

Approximate quantum mechanical solutions can be obtained if the shape of the potential well is simplified. Assuming a homogeneous channel doping it can be shown that the potential may be approximated as, $V(z) = \xi z$ (triangular approximation) with ξ the normal electric field due to the charge in the depletion layer. Triangular potential well approximation, so called because the potential well is bounded on one side by the vertical barrier that keeps electrons out of the insulation and on the other side by the linearly rising potential.

In this chapter, in order to determine the expressions for the energy sub-bands of the potential well, the Schrödinger wave equation is solved with the condition that the envelope wave function goes to zero at $z = 0$ and at infinity. The solutions are Airy functions [8]. Only the first two consecutive sub-bands are taken. The average separation of carriers in the two-subbands from the surface is then calculated by using the standard method of integration. By using Fermi-Dirac statistical distribution law the carrier

population in the two sub-bands are also determined. Knowing the carrier concentration in the sub-bands, an analytical expression for capacitance is determined by simply differentiating the total charge in the inversion layer with respect to the surface potential.

2.2 Sub-bands of a triangular potential well

2.2.1 Airy function approximation

This is an approximate method of solution of ordinary differential equation and is useful for the approximate solution of quantum-mechanical problems [8].

2.2.2 Triangular potential approximation

In the MOSFET structure the width of the inversion layer is in the nanometer range for high substrate doping levels, so the electrostatic potential of the well can be assumed to be triangular. The depth of the potential well at the Si/SiO₂ interface is approximately several electron volts, so it can be assumed as infinite potential wall.

2.2.3 Approximate solution

The potential energy of the particle under consideration is of the form

$$V(z) = \begin{cases} \infty & ; z \leq 0, \\ eF_0 z & ; z \geq 0. \end{cases}$$

where the direction z is taken along the positive z -axis and where $z = 0$ is the reflecting plane.

This potential energy and also the energy levels and wave functions which we shall obtain are depicted in (Fig.2.1). We restrict ourselves to an investigation of the motion of the particle in the z -direction since the motion in the xy -plane is free and is of no interest at the moment. The time-independent Schrödinger equation for the particle wave function $\psi(z)$ in the region $z \geq 0$ is then:

$$\frac{d^2\psi}{dz^2} + \frac{2m_e}{\hbar^2} (E - eF_0 z) \psi = 0 \quad (2.1)$$

where E is the particle energy. This equation must be solved with the boundary conditions

$$\psi \rightarrow 0 \quad \text{as} \quad z \rightarrow \infty \quad (2.2)$$

and

$$\psi = 0 \quad \text{for} \quad z = 0 \quad (2.3)$$

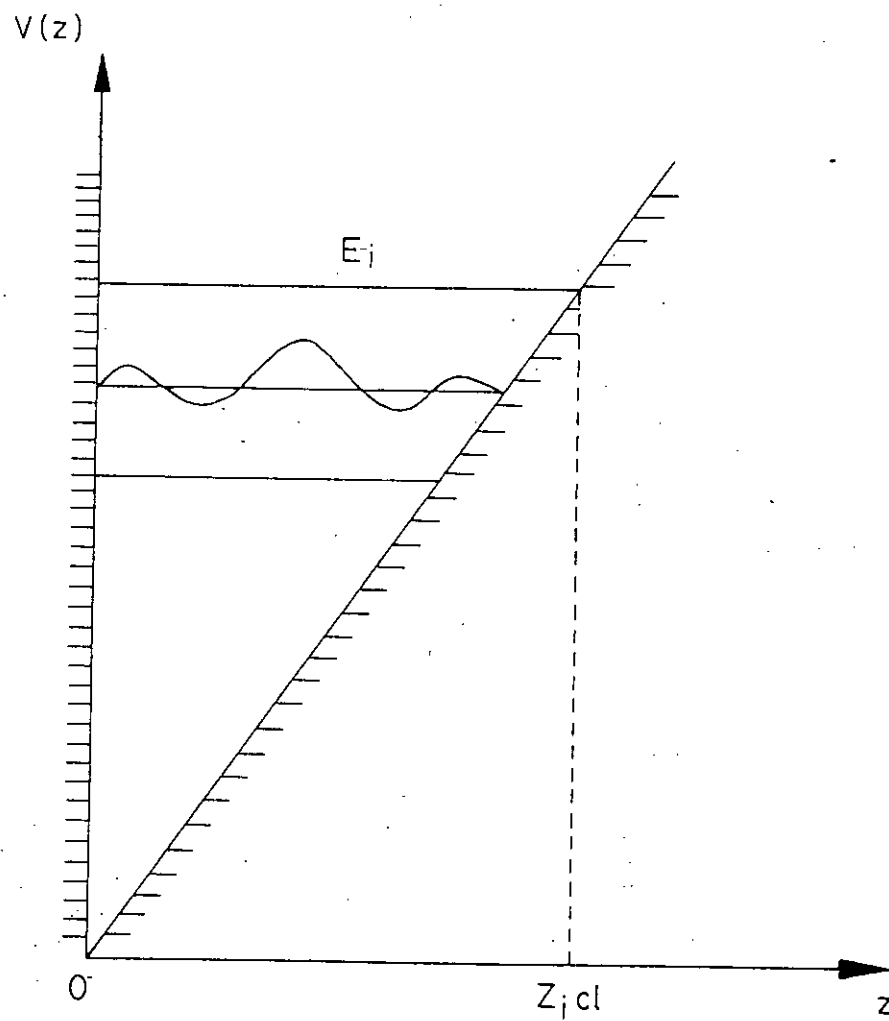


Fig. 2.1 Energy sub-bands in a triangular potential well.

To simplify equation (2.1) we introduce a new independent variable ξ which is connected with z by the relation

$$\frac{2m_z e F_s}{\hbar^2} z - \frac{2m_z}{\hbar^2} E = c\xi \quad (2.4)$$

where c is for the moment an arbitrary constant,

Substituting this variable c into equation (2.1) transforms it to

$$\frac{d^2 \Psi}{d\xi^2} - c^3 \left(\frac{\hbar^2}{2m_z e F_s} \right)^2 \xi \Psi(\xi) = 0 \quad (2.5)$$

It is now clear that if we take

$$c = \left(\frac{2m_z e F_s}{\hbar^2} \right)^{\frac{2}{3}},$$

that is, write equation (2.4) in the form

$$\xi = \left(\frac{2m_z e F_s}{\hbar^2} \right)^{\frac{1}{3}} \left(z - \frac{E}{e F_s} \right) \quad (2.6)$$

we are led to the very simple form, putting the value of c in (2.8),

$$\Psi''(\xi) - \xi \Psi(\xi) = 0 \quad (2.7)$$

The solution of this equation which is finite for all values of ξ , that is, also for all value of z , is

$$\psi = A \phi(\xi) \equiv A \frac{1}{\sqrt{\pi}} \int_0^{\xi} \cos(\xi t + \frac{1}{3} t^3) dt \quad (2.8)$$

where $\phi(\xi)$ is the Airy function and A is a normalization factor

It is clear that the energy levels of a particle which is in the potential well shown in (Fig.2.2), form a discrete spectrum and their number is infinite. To find these levels we use the boundary condition (2.3); $\psi = 0$ for $z = 0$, in equation (2.6), that is ,

$$\xi = \left(\frac{2m_z e F_s}{\hbar^2} \right)^{\frac{1}{3}} \left(- \frac{E}{e F_s} \right)$$

or

$$\xi = \left(- \frac{2^{\frac{1}{3}} m_z^{\frac{1}{3}}}{e^{\frac{2}{3}} F_s^{\frac{2}{3}} \hbar^{\frac{2}{3}}} E \right)$$

and from equation (2.8) we have, $\psi = A \phi(\xi) = 0$ or

$$\phi \left(- \frac{2^{\frac{1}{3}} m_z^{\frac{1}{3}}}{e^{\frac{2}{3}} F_s^{\frac{2}{3}} \hbar^{\frac{2}{3}}} E \right) = 0 \quad (2.9)$$

Putting the argument of equation (2.9) equal to the roots of the Airy function which we shall define by $-a_i$, ($i=1,2,\dots$)

$$0 < a_1 < a_2 < \dots < a_i < \dots$$

we find for the solutions E_i of this transcendental equation.

$$-\left(\frac{2m_z}{e^2 F_s^2 \hbar^2}\right)^{\frac{1}{3}} E_i = -\alpha_i \quad (2.10)$$

Hence, the required energy spectrum of the potential has the form

$$E_i = \left(\frac{e^2 F_s^2 \hbar^2}{2m_z}\right)^{\frac{1}{3}} \alpha_i \quad (i = 1, 2, 3, \dots) \quad (2.11)$$

The wave functions of the corresponding stationary states can also be found. From equation (2.6) and (2.8) we have,

$$\psi_i(z) = A_i \phi\left[\left(\frac{2m_z e F_s}{\hbar^2}\right)^{\frac{1}{3}} \left(z - \frac{E_i}{e F_s}\right)\right]$$

Then putting the value of E_i from equation 2.11 in the above equation we have,

$$\begin{aligned} \psi_i(z) &= A_i \phi(-\xi_i) \\ &= A_i \phi\left(\frac{z}{a} - \alpha_i\right) \end{aligned} \quad (2.12)$$

In this equation 'a' denotes characteristic length.

$$a = \left(\frac{\hbar^2}{2m_z e F_s}\right)^{\frac{1}{3}} \quad (2.13)$$

The normalizing factor A depends on i and a. As the Airy function is real for real values of its argument, we have

$$|\phi(\xi)|^2 = [\phi(\xi)]^2 \quad (2.14)$$

The constant factor in equation (2.12) is determined from the normalization of ψ .

If we normalize (2.12) with respect to ξ

$$\int_{-\infty}^{\infty} |A\phi(\xi_i)|^2 d\xi = \int_{-\infty}^{\infty} [A\phi(\xi_i)]^2 d\xi = 1$$

or,

$$A_i = \frac{1}{\sqrt{\int_{-\infty}^{\infty} [\phi(\xi)]^2 d\xi}} \quad (2.15a)$$

and if we normalize with respect to z , constant in clearly equal to,

$$A_i = \frac{1}{\sqrt{a}} \frac{1}{\sqrt{\int_{-\infty}^{\infty} [\phi(\xi)]^2 d\xi}} \quad (2.15b)$$

We investigate now the asymptotic behavior of the wave functions $\psi_i(z)$ at sufficiently large distances from the classical turning point, z_i^{cl} , and also the form of the energy E_i for $i \geq 1$. z_i^{cl} is the greatest height which a classical particle of given energy E_i can attain, which is,

$$z_i^{cl} = \frac{E_i}{eF_s} \quad (2.16)$$

According to the equation (2.11) and (2.13) the lengths z_i^{cl} and 'a' are connected by the relation

$$z_i^{cl} = a \alpha_i \quad (2.17)$$

we use equations (2.13), (2.16) and (2.17) to write equation (2.6) in the form

$$\xi = \frac{z - z_i^{cl}}{a} = \frac{z}{a} - \alpha_i \quad (2.18)$$

and consider the asymptotic expressions for the functions $\psi_i(z)$.

Case (1): For the classically inaccessible region and values of z not too near z_i^{cl} :

$$z - z_i^{cl} \gg a \text{ i.e., } \xi \gg 1$$

Now using the asymptotic expression for the Airy function of the following form:

$$\phi(\xi) \approx \frac{1}{2\xi^{\frac{1}{4}}} \exp\left(-\frac{2}{3}\xi^{\frac{3}{2}}\right) \quad (2.19)$$

which can be written in the following form using equations (2.12) and (2.18);

$$\psi_i(z) \approx \frac{A_i}{2} \left(\frac{a}{z - z_i^{cl}}\right)^{\frac{1}{4}} \exp\left[-\frac{2}{3} \left(\frac{z - z_i^{cl}}{a}\right)^{\frac{3}{2}}\right] \quad (2.20)$$

From the above equation we can conclude that there is exponential decrease of the probability $|\psi_i(z)|^2$ in the classically inaccessible region.

Case (2): For the region of classical motion and values of z not too near z_i^{cl} :

$$0 < z < z_i^{cl} \quad |z - z_i| \gg a,$$

that is ,

$$-\alpha_i < \xi < 0$$

and

$$|\xi| \gg 1$$

It is clear that to satisfy the second condition at least the following inequality must be obtained :

$$a_i \gg 1$$

The required asymptotic expansion of the Airy function has of the form:

$$\phi(\xi) = \frac{1}{|\xi|^{\frac{1}{4}}} \sin \left(\frac{2}{3} |\xi|^{\frac{3}{2}} + \frac{\pi}{4} \right) \quad (2.21)$$

Using equations (2.12) and (2.18) we have,

$$\psi_i(z) = A_i \left(\frac{a}{|z - z_i^{cl}|} \right)^{\frac{1}{4}} \sin \left[\frac{2}{3} \left(\frac{|z - z_i^{cl}|}{a} \right)^{\frac{3}{2}} + \frac{\pi}{4} \right] \quad (2.22)$$

The asymptotic expressions (2.20) and (2.22) give us in this way the semiclassical wave functions. By means of (2.22) one can find explicit expressions for the roots of the Airy function $\xi_i = -\alpha_i$, and hence also for the energy levels (2.11) in the semi-classical case.

To do this we must clearly equate the argument of the sine to an integral multiple of π :

$$\frac{2}{3} |\xi|^{3/2} + \frac{\pi}{4} = (i+1)\pi$$

$$i = 0, 1, 2, 3, \dots$$

So that,

$$\begin{aligned} \alpha_i &= |\xi_i| \\ &= \left[\frac{3}{2} (i+1)\pi - \frac{3}{2} \frac{\pi}{4} \right]^{2/3} \\ &= \left[\frac{3}{2} \left(i\pi + \frac{3\pi}{4} \right) \right]^{2/3} \end{aligned} \quad (2.23)$$

and from equation (2.11) we get, [3]

$$E_i = \left(\frac{\hbar^2}{2m_g} \right)^{1/3} \left[\frac{3}{2} \pi e F_g \left(i + \frac{3}{4} \right) \right]^{2/3}$$

$$i = 0, 1, 2, 3, \dots$$
(2.24)

This is the required analytical expression for energy subbands in the inversion layer of MOSFETS.

Taking only the ground and first sub-bands by putting $i=0$ and $i=1$ we find the following expressions.

$$E_0 = 8.03916 \times 10^{-7} (F_s)^{2/3} \text{ eV}$$

$$E_1 = 1.4142582 \times 10^{-6} (F_s)^{2/3} \text{ eV}$$

Where F_s is in V/m.

2.3 Population of carriers in the two sub-bands

The density-of-states for a two-dimensional system is constant and is given by the following equation [3].

$$D = \frac{n_v m_d}{\pi \hbar^2} g \left(\frac{1}{m^2 V} \right) \quad (2.25)$$

Here, n_v and m_d are the valley degeneracy factor and the density-of-states effective mass per valley.

For a two-dimensional density-of-states given by D between E_0 and E_1 and equal to $2D$ for energies greater than E_1 , we have, the total electron population taking two subbands into account,

using, Fermi-Dirac Statistics:

$$N_{inv} = D \int_{E_0}^{E_1} \frac{dE}{1 + e^{\frac{(E - E_F)}{kT}}} + 2D \int_{E_1}^{\infty} \frac{dE}{1 + e^{\frac{(E - E_F)}{kT}}} \quad (2.26)$$

Using the integration formula,

$$\int \frac{dx}{1 + e^x} = -\ln(1 + e^{-x})$$

we obtain,

$$N_{inv} = DkT \ln \left[\left(1 + e^{\frac{(E_F - E_0)}{kT}} \right) \left(1 + e^{\frac{(E_F - E_1)}{kT}} \right) \right] \quad (2.27)$$

Therefore,

$$N_{inv} = \sum_i N_i$$

is the total number of charges per unit area in the inversion layer.

2.4 Average separation of minority carriers from the interface.

The average distance from the semiconductor-insulator interface of the electrons in the i th sub-band is defined by

$$Z_i = \frac{\int_0^{\infty} z \phi_i^2(z) dz}{\int_0^{\infty} \phi_i^2(z) dz} \quad (2.28)$$

Using (2.22), equation (2.28) reduces to

$$Z_i = \frac{2E_i}{3qF_s} \quad (2.29)$$

Z_{av} is the average penetration of all the inversion layer charge from the surface which is given by

$$Z_{av} = \sum_i \frac{N_i Z_i}{N_{inv}} \quad (2.30)$$

2.5 An analytical expression for inversion layer quantum capacitance

During carrier depletion the total charge per unit area Q_s is given by [9]

$$Q_s = Q_b = -qN_A z_d$$

where, z_d is the depletion layer width Q_b denotes the bulk charge in the semiconductor. The relationship between ψ_s and z_d can be obtained by solving Poissons equation using the depletion approximation. The result is [9]:

$$Z_d = \sqrt{\frac{2\epsilon_s \psi_s}{qN_a}}$$

When $\psi_s > 2\phi_f$, since the increase of ψ_s is added to the difference of E_f and E_i , a small increase of ψ_s produces a large increase of electrons at the surface, from (1.4) according to the exponential nature of the equation. Therefore, the surface inversion layer is acting like a narrow n^+ layer and the induced junction resembles an n^+p junction for a large positive gate voltage. However, all induced charge will be in the inversion layer after strong inversion and the charge inside the depletion layer will remain constant. Thus, the space-charge width remains at z_{dn} as we further increase the gate voltage i.e.

$$Q_B = -qN_A z_{dn}$$

and

$$z_{dn} = \sqrt{\frac{2\epsilon_s \psi_{si}}{qN_A}} \quad (2.31)$$

A small increase in the gate voltage increases the silicon surface potential ψ_s so that holes are depleted and the depletion layer is widened. Therefore more negative fixed

charge is established at the edge of the neutral p-type semiconductor as shown in (Fig.2.2a).

If we assume now that electron-hole pairs can be generated fast enough, the generated holes will replenish the depleted holes at the edge of the depletion region. At the same time, the generated electrons will be drawn by the field and accumulate at the Si-SiO₂ interface (Fig.2.2b). To determine the inversion layer capacitance let us, therefore, assume that the depletion width z_d and charge remain essentially constant after carrier depletion.

Now, z_d is given by,

$$Z_d = \sqrt{\frac{2e_s \phi_d}{qN_A}} \quad (2.32)$$

where ϕ_d is the effective band bending from the bulk to the surface, apart from the contribution of the inversion layer itself, is given by (Fig.2.3),

$$q\phi_d \approx (E_C - E_F)_b \quad (2.33)$$

and

$$N_{depl} = N_A Z_d \quad (2.34)$$

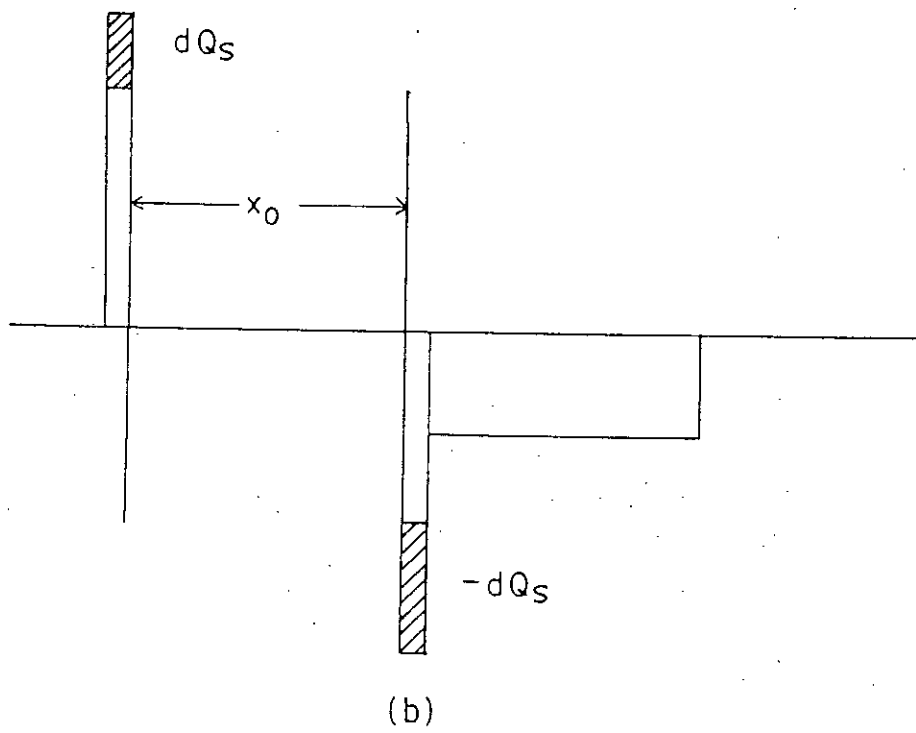
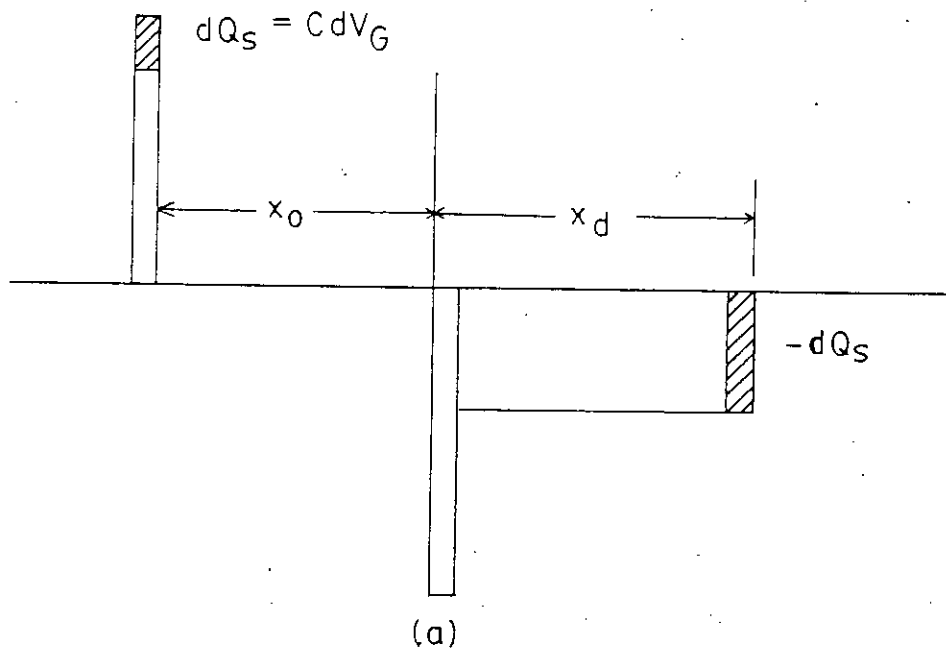
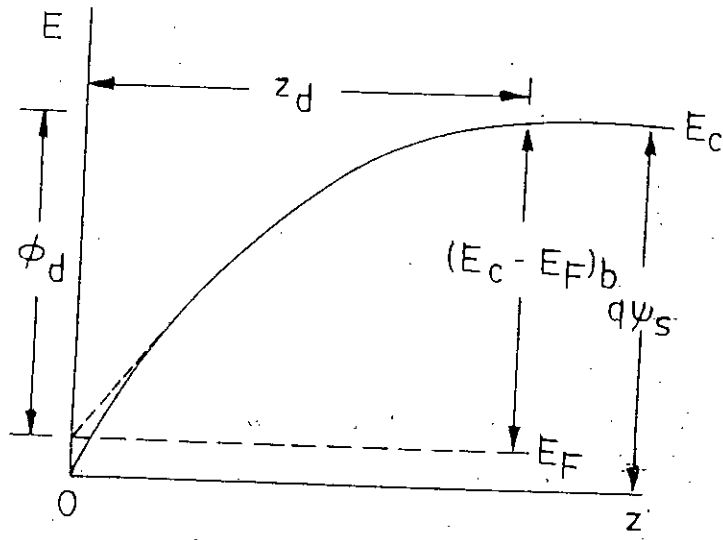
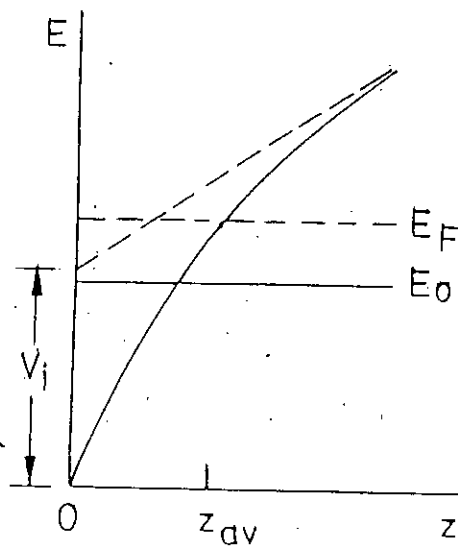


Fig. 2-2 Charge distribution in a MOS capacitor.
 (a) Depletion layer charge
 (b) Inversion layer charge.



(a)



(b)

Fig. 2.3 Band bending due to depletion charges.
 (a) Surface potential ψ_s and band bending
 (b) Potential drop due to inversion charges

is the number of charges per unit area in the depletion layer and $N_{inv} = \sum N_i$, is the total number of charges per unit area in the inversion layer.

The electric field F_s is given by,

$$F_s = \frac{q}{\epsilon_s} (N_{inv} + N_{depl}) \quad (2.35)$$

Field vanishes for large z and its value at the surface be F_s .

Here we have assumed that the depletion charge is constant for a distance z_d from the surface and then goes abruptly to zero. But actually charge density decays smoothly. This effect can be accounted for by adding a constant to the band bending used to calculate z_d in equation (2.32).

The correction to ϕ_d is taken to be $-kT/q$ [3]

$$q\phi_d = [(E_c - E_F)_b + E_F - kT] - \frac{N_{inv} Z_{av}}{\epsilon_s} \quad (2.36)$$

where the first term $(E_c - E_F)_b$ is the energy difference between the bottom of the conduction band in the bulk and the Fermi level. E_F is the Fermi energy relative to the nominal conduction band edge at the surface. $(E_c - E_F)_b$ is given by

$$(E_c - E_f)_b = \frac{E_g}{2} + kT \ln \frac{N_A}{n_i} \quad (2.37)$$

The last term in equation (2.36) is the potential drop across the inversion layer, V_i , due to the inversion layer charges. From equation (2.36) we can write

$$\psi_s = \phi_d + \frac{kT}{q} + q \frac{N_{inv} Z_{av}}{e_s} \quad (2.38)$$

Inversion layer quantum capacitance is denoted by

$$C_{inv} = - \frac{dQ_{inv}}{d\psi_s} \quad (2.39)$$

Q_{inv} is the total charge in the inversion layer and ψ_s is the surface potential.

Putting $Q_{inv} = - qN_{inv}$ in equation (2.38) we have,

$$C_{inv} = q \frac{dN_{inv}}{d\psi_s} \quad (2.40)$$

Now from equation (2.27) we can write,

$$N_{inv} = N_0 + N_1 \quad (2.41)$$

where,

$$N_0 = DkT \ln \left(1 + e^{\frac{(E_f - E_0)}{kT}} \right) \quad (2.41a)$$

and

$$N_1 = DkT \ln \left(1 + e^{\frac{(E_F - E_1)}{kT}} \right) \quad (2.41b)$$

Assume,

$$u_0 = e^{\frac{(E_F - E_0)}{kT}}$$

$$u_1 = e^{\frac{(E_F - E_1)}{kT}}$$

and $E_0 = a F_s^{2/3}$

$E_1 = b F_s^{2/3}$

where a and b are adjustable parameters .

Differentiating equation (2.30) with respect to F_s we have,

$$\frac{dN_{inv}}{dF_s} = DkT \left(-\frac{1}{kT} \right) \frac{2}{3} F_s^{-1/3} \left[\frac{au_0}{1+u_0} + \frac{bu_1}{1+u_1} \right] \quad (2.42)$$

And differentiating equation (2.38) with respect to F_s (assuming that ϕ_i is fixed after the inversion layer begins to form) we have,

$$\frac{d\psi_s}{dF_s} = \frac{d}{dF_s} \left(q \frac{N_{inv} Z_{av}}{e_s} \right)$$

where Z_{av} is given by equation (2.30). Using equations (2.26), (2.41a) and (2.41b) we get,

$$\begin{aligned} \frac{d\psi_s}{dF_s} = DkT \frac{2}{3} \frac{1}{e_s} \frac{2}{3} \left(-\frac{1}{kT}\right) F_s^{-\frac{2}{3}} \left(\frac{a^2 u_0}{1+u_0} + \frac{b^2 u_1}{1+u_1} \right) \\ + \left(-\frac{1}{3}\right) F_s^{-\frac{4}{3}} \{ a \ln(1+u_0) + b \ln(1+u_1) \} \end{aligned} \quad (2.43)$$

Dividing equation (2.42) by (2.43) and multiplying by q we get the inversion capacitance i.e.,

$$\begin{aligned} q \left(\frac{dN_{inv}}{dF_s} \frac{dF_s}{d\psi_s} \right) \\ = q \frac{dN_{inv}}{d\psi_s} \\ = C_{inv} \end{aligned}$$

Thus the inversion layer quantum capacitance is given by,

$$C_{inv} = \frac{\frac{3}{2} e_s F_s \left[\frac{a u_0}{1+u_0} + \frac{b u_1}{1+u_1} \right]}{\left[F_s^{\frac{2}{3}} \left(\frac{a^2 u_0}{1+u_0} + \frac{b^2 u_1}{1+u_1} \right) + 2kT(a \ln(1+u_0) + b \ln(1+u_1)) \right]} \quad (2.44)$$

The inversion layer quantum capacitance depends upon the electric field F_s and eigen energy of two sub-bands. The algorithm for finding C_{inv} is developed in chapter 3.

2.6 Summary

In this chapter, an analytical expression for inversion layer quantum capacitance is derived. The populations of electrons in two sub-bands are determined using density of states and Fermi-Dirac statistics. Knowing the electron population and average separation of minority carriers from the interface, an expression for surface potential ψ_s is established in this chapter. The total charge of the carriers Q_{inv} , in the two sub-bands are shown as a function of surface potential. Derivative of Q_{inv} with respect with ψ_s gives C_{inv} .

CHAPTER 3

RESULTS BASED ON ANALYTICAL SOLUTION

3.1 Introduction

A MOS-capacitor is studied using computational method. The analytical model developed in chapter 2 is used here to determine the inversion layer capacitance considering quantum effects. One dimensional searching algorithm is used in the computational method. The inversion layer charge density, the eigen energies obtained using different approximations, the average separation of carriers from the surface, the carrier concentration in two consecutive sub-bands and finally, the classical and quantum mechanical inversion region gate capacitance for a MOS capacitor have been compared in this study.

3.2 Computational method in studying the MOS device.

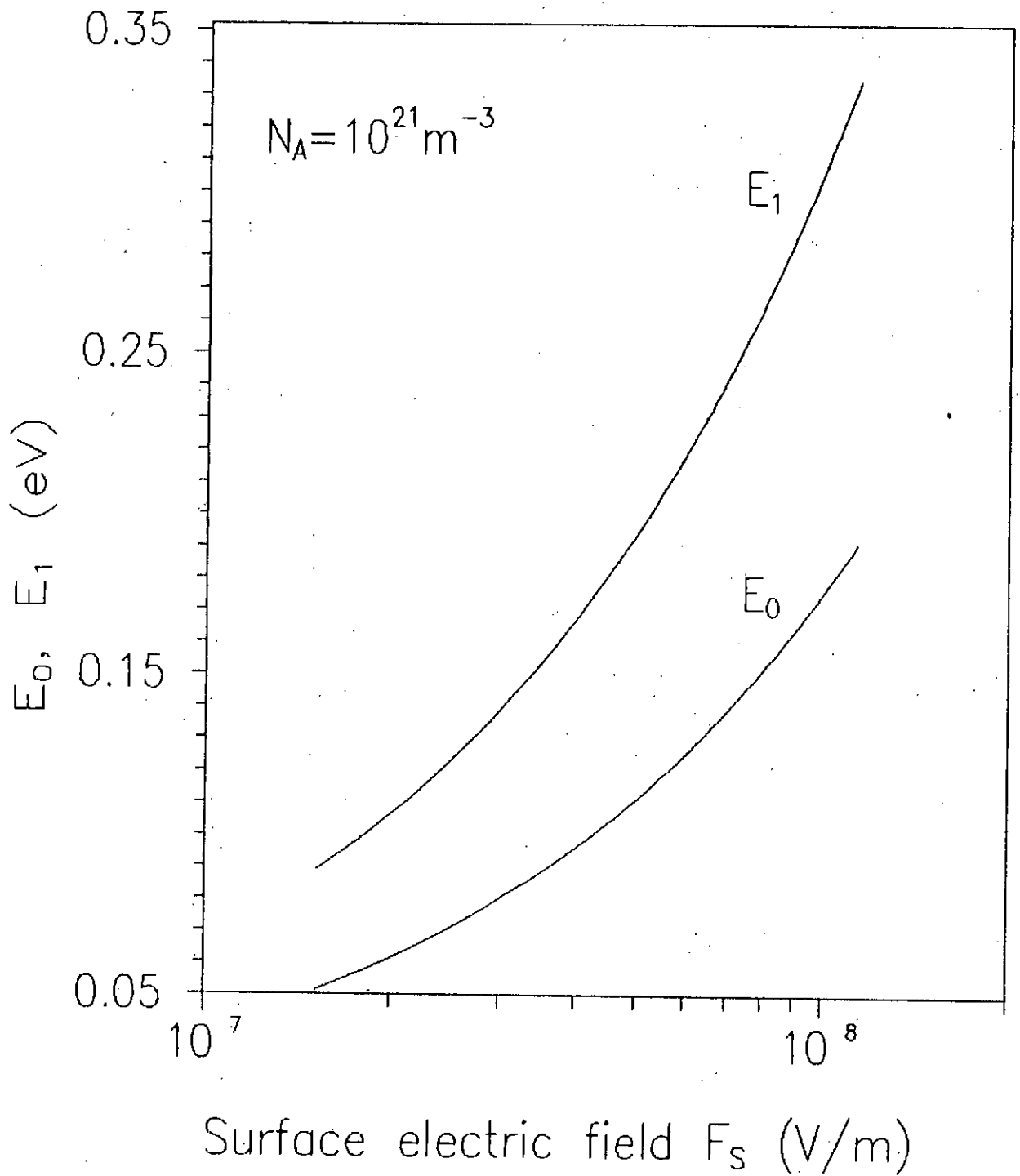
The classical inversion layer capacitance is calculated

by using equation (1.13). First we assumed the surface electric field to be F_{s1} (V/m). The lower and the first energy sub-bands E_0 and E_1 respectively were calculated using equation (2.24). The inversion layer charge N_{inv1} (m^{-3}) is then assumed and using a one dimensional searching algorithm E_f i.e., the position of the Fermi level is determined. Knowing E_f we can now calculate ϕ_d from equation (2.36), z_d from equation (2.32) and the depletion layer charge N_{depl} from equation (2.34). A new value of electric field F_{s2} is then found from the sum of the inversion and the depletion layer charges given by equation (2.35). When F_{s1} and F_{s2} matches then the searching algorithm comes to an end. For a particular value of F_s , then the corresponding Fermi energy level (E_f), surface potential (ψ_s), the lowest and the first energy levels (E_0 and E_1) are determined. Finally using equation (2.44) the inversion layer quantum capacitance C_{inv} is calculated.

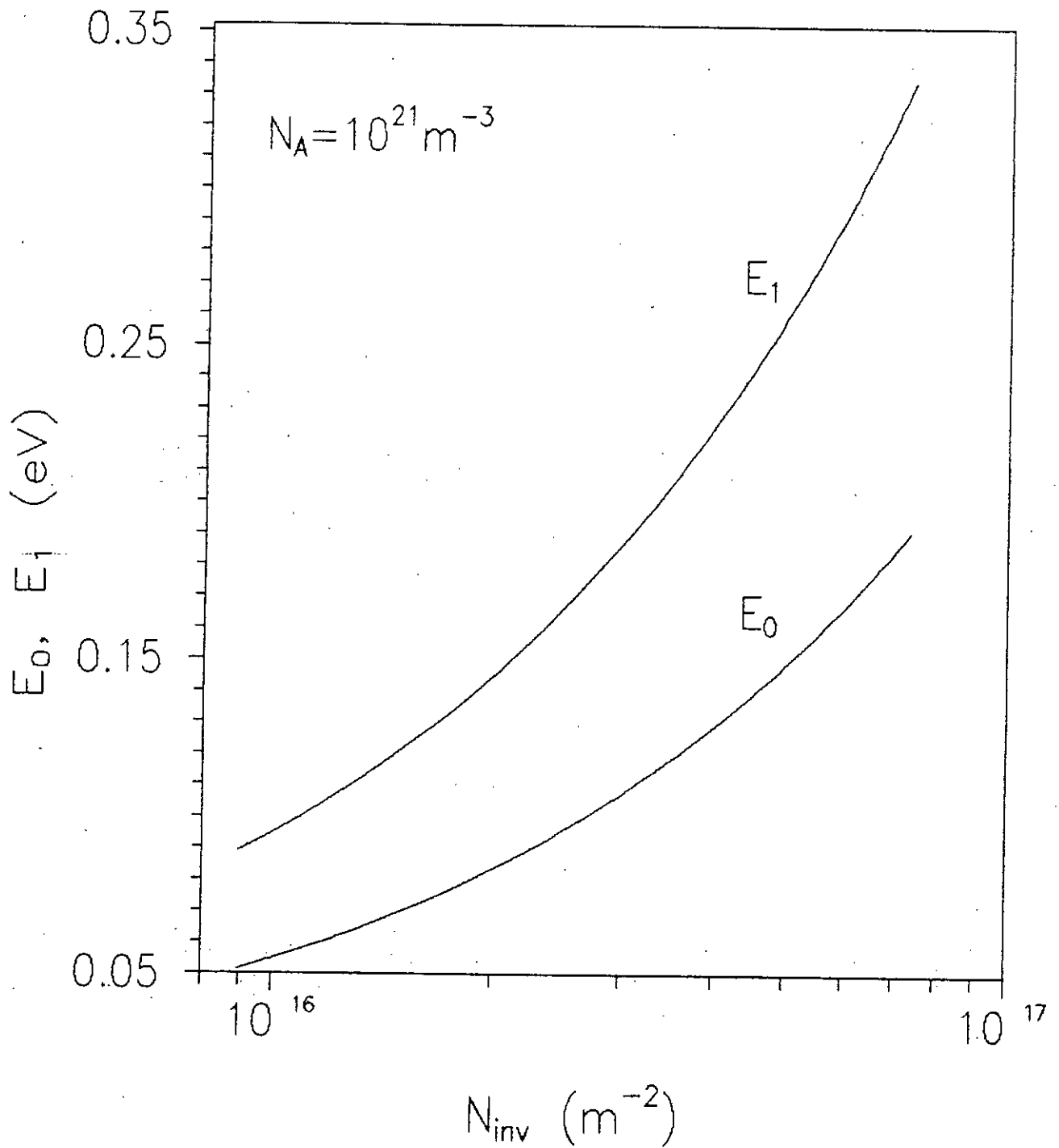
3.3 Results and discussions

3.3.1 Quantization of Energy levels

The predicted energy levels of the lower two-subbands (E_0 and E_1) for a MOS capacitor with a gate oxide thickness 10nm and with a uniform channel doping of $N_A = 10^{21} m^{-3}$ is shown in (Fig.3.1 and Fig.3.2). The energy levels of the lower two-subbands (E_0 and E_1) increases as the device becomes more strongly inverted.



Plots of
 Fig. 3.1 Effect of surface electric field on the energy levels.



Plots of
 Fig. 3.2 Energy levels vs. inversion layer charge.

3.3.2 Inversion layer charge concentration

(Fig.3.3) shows the inversion layer charge concentration for a uniform channel doping of 10^{21} m^{-3} and for a gate oxide thickness of 10nm. The inversion layer charge concentration (N_{INV}) increases with the surface potential (ψ_s).

3.3.3 Depletion layer charge concentration

From (Fig.3.4) we find that the variation of depletion layer charge with the surface potential is very small compared to the inversion layer charge concentration. After strong inversion, a small increase of ψ_s produces a large increase of electrons at the surface and the inversion layer acts like a narrow n^+ layer by shielding the semiconductor from further penetration of the electric field. Therefore the depletion layer charge remains constant and after strong inversion the depletion layer width becomes fixed at Z_{dn} .

3.3.4 Electron Concentrations in the two sub-bands

The electron distribution in the two sub-bands as a function of the applied surface potential is shown in (Fig.3.5). Here we

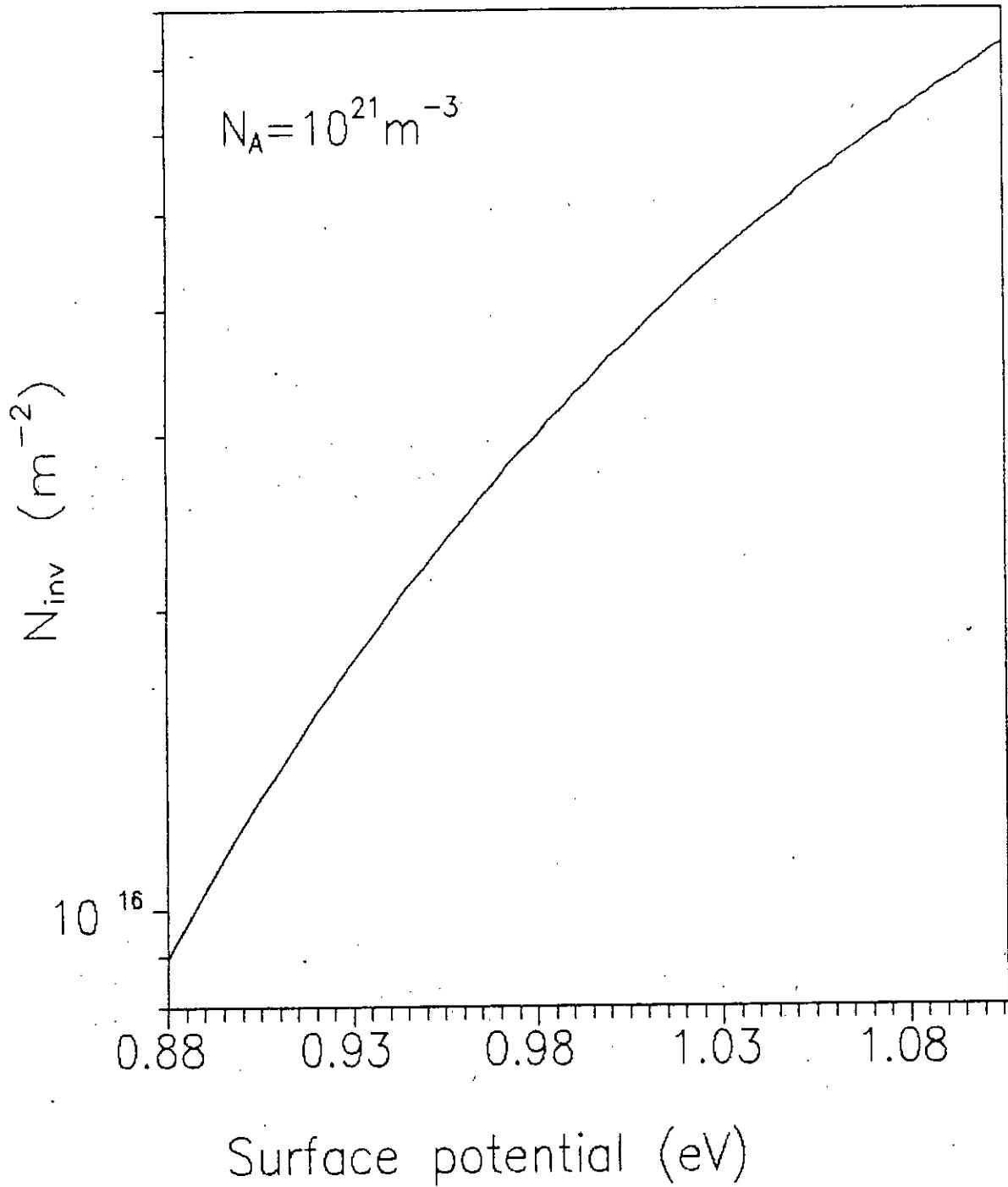


Fig. 3.3 Effect of surface potential on inversion layer charge.

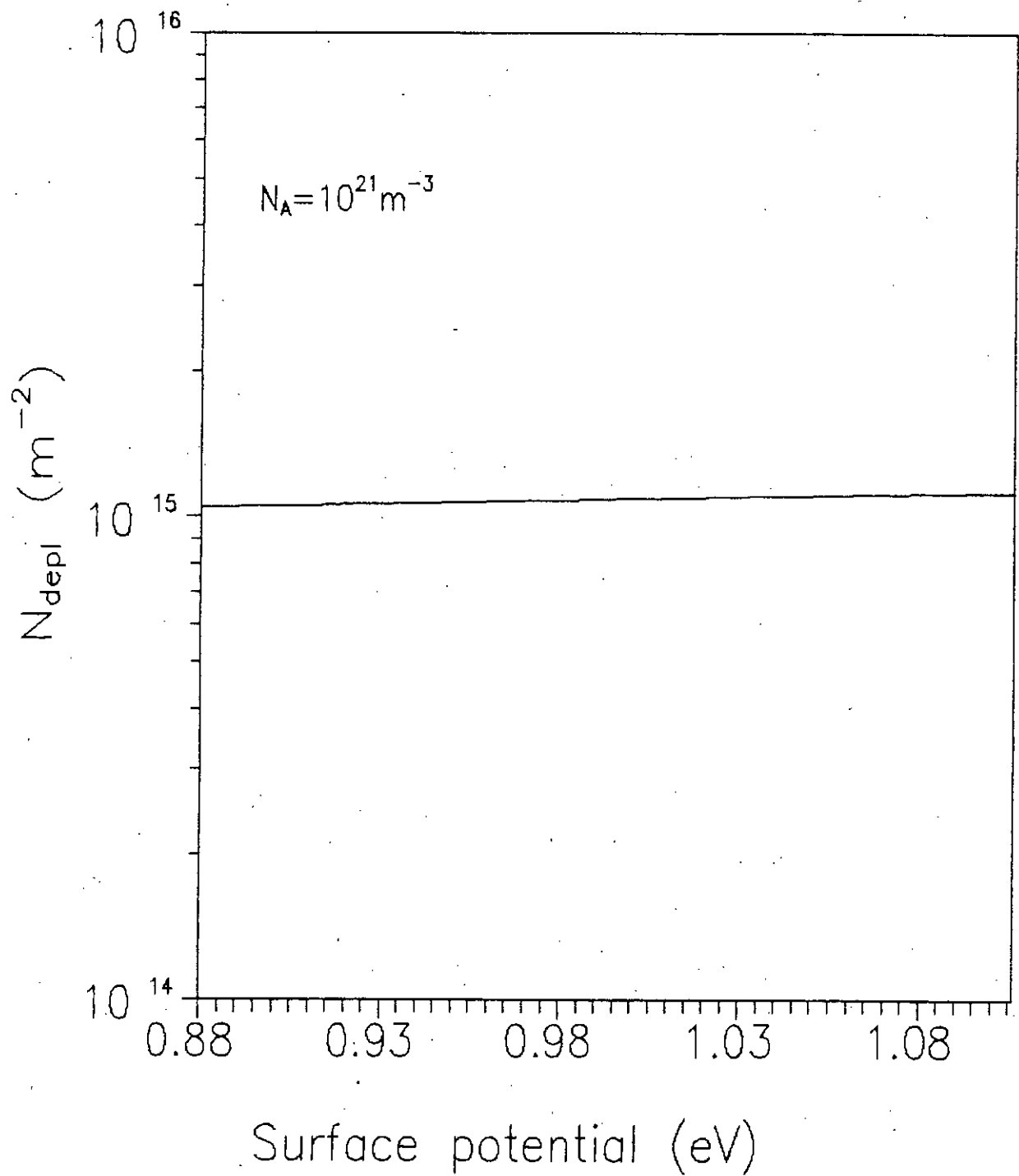


Fig. 3.4 Effect of surface potential on depletion layer charge.

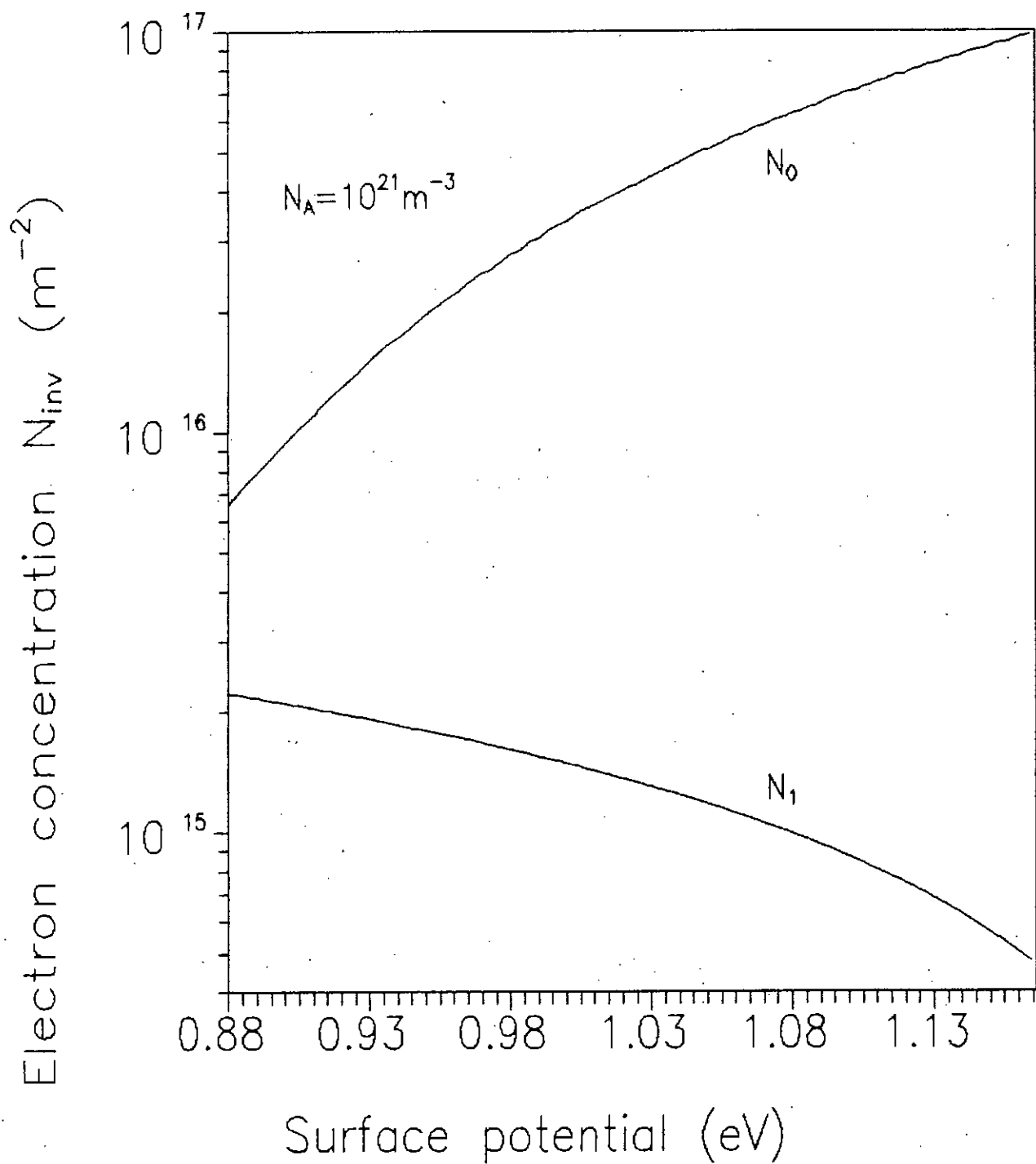


Fig. 3.5 Electron concentration of the two sub bands vs. surface potential.

observe that, as ψ_s increases the electron concentration in the lowest sub-band increases whereas the electron concentration in the first sub-band decreases. This can be explained from (Fig.3.1) where we find that as ψ_s increases the difference between E_0 and E_1 increases i.e., the probability for the electrons to occupy the lowest sub-band also increases.

3.3.5 Average spatial extent of the inversion layer electrons from the surface.

The average penetration of the inversion layer charge density from the surface Z_{av} as a function of the inversion layer charge concentration and the surface potential for p-type silicon with 10^{21} acceptors per m^{-3} in the bulk at 300K is shown in (Fig.3.6 and Fig.3.7) respectively. The decrease of Z_{av} with increasing inversion layer charge is a reflection of the increasing surface electric field seen by the electrons which pushes them closer to the surface.

3.3.6 Inversion layer capacitance:

The predicted difference between quantum mechanically and classically calculated capacitance in inversion for an MOS capacitance with a gate oxide thickness of 10nm and a uniform channel doping of $10^{21} m^{-3}$ is shown in (Fig.3.8). From figure we

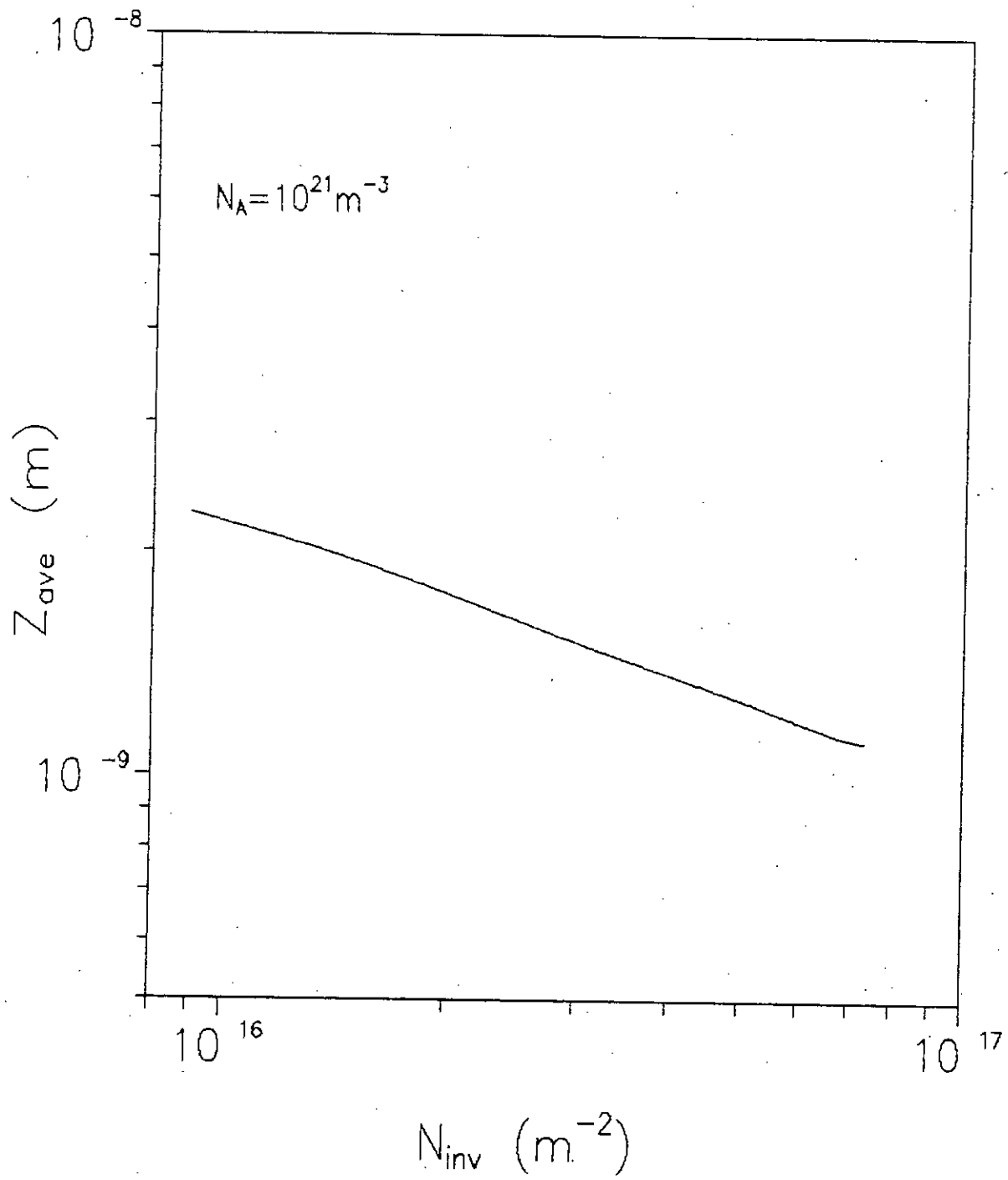


Fig. 3.6 Average separation of carriers vs. inversion layer charge.

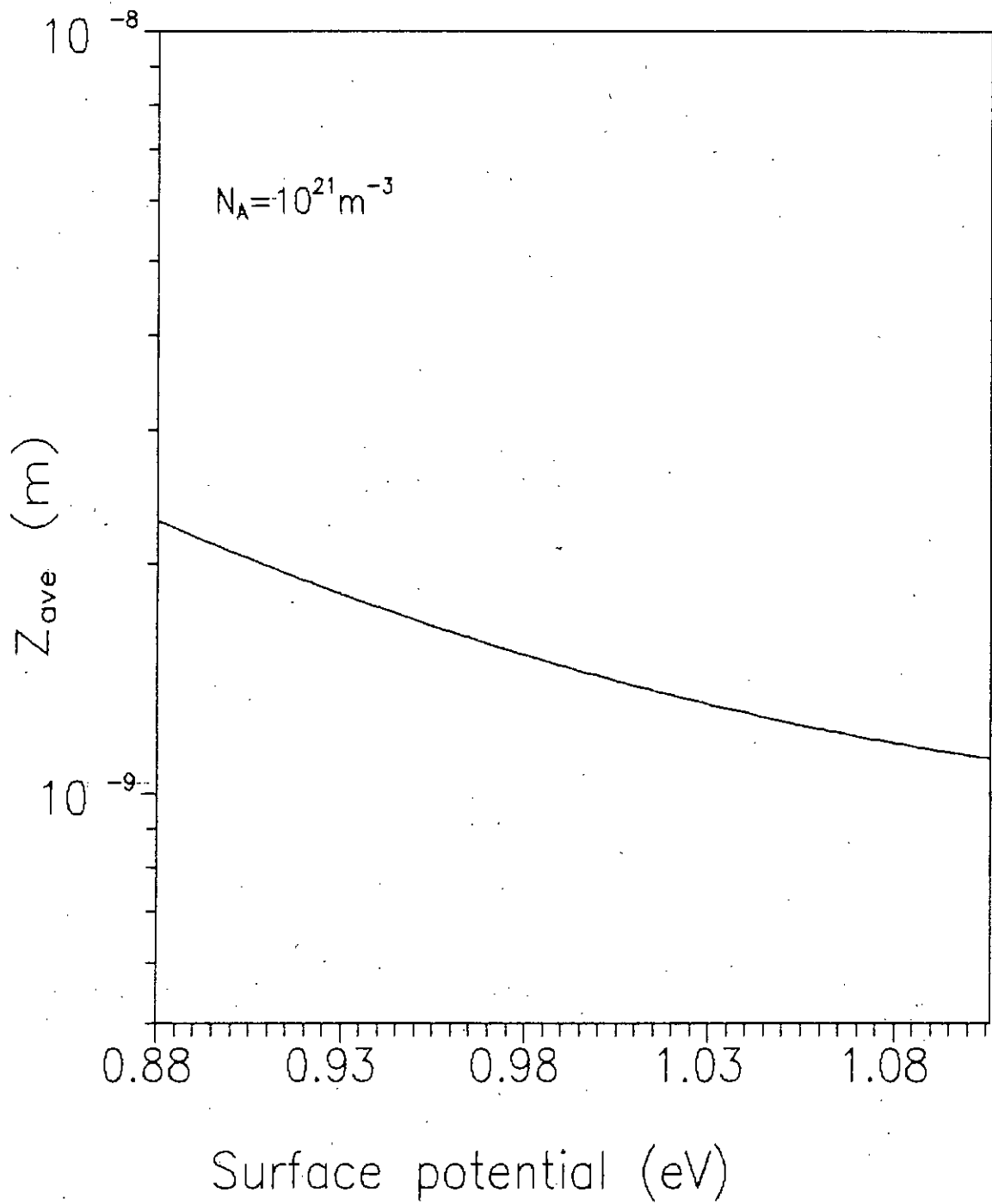


Fig. 3-7 Average separation of carriers vs. surface potential.

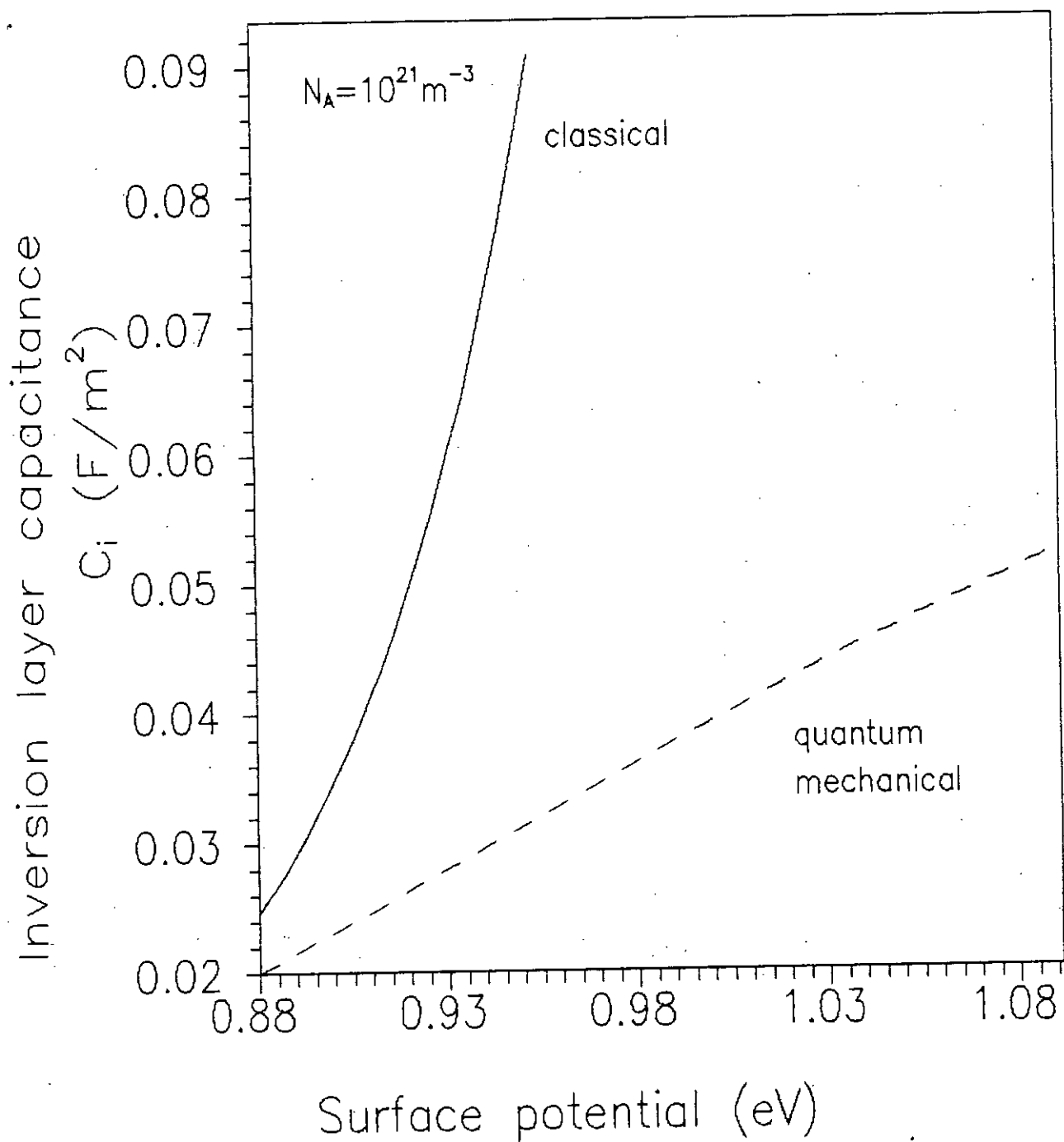


Fig. 3.8 Effect of surface potential on the classical and quantum mechanical capacitances.

find that, the difference between the predicted inversion layer capacitance when the quantum mechanical effects are included with that calculated classically increases markedly when surface potential is increased. The variation of inversion layer quantum capacitance with the applied surface potential is small because with the increase of ψ_s , the energy levels E_0 and E_1 shifts upward and the number of inversion layer carriers cannot increase at the previous rate which is exponential in nature. Therefore for a given value of surface potential the inversion layer capacitance calculated quantum mechanically will be smaller than when calculated classically.

3.4 Summary

The analytical model developed in chapter 2 is used here to determine the inversion region quantum capacitance of the MOS-capacitor. The approach of the analysis and the computational method is also described.

The variations of the energy levels and the inversion layer charge concentration with the applied surface potential and electric field are studied and are found to be increasing in nature.

The depletion layer charge concentration varies but very slightly with the surface potential.

The electron concentration in the two sub-bands is studied

and is seen that most of the carriers occupy the lowest energy level with the increasing gate voltage.

The average separation of the inversion layer electrons from the interface decreases with the applied field.

Finally, the variation of the inversion layer quantum capacitance with the applied surface potential is studied and is found to be small compared to the classical one.

CHAPTER 4

CONCLUSIONS

4.1 Conclusions

In this work an analysis is presented to determine the inversion layer capacitance of MOSFETs incorporating quantum mechanical effects.

The Schrödinger wave equation is solved by using triangular potential approximation which leads to the Airy equation. From the solution we find the eigen energy equation E_i from which only the first two consecutive subbands are considered. The average separation of carriers in the two subbands from the surface is calculated by using the standard method of integration. The Fermi-Dirac statistical law gives the carriers population in the two subbands. From the equations of separation of carriers and the carrier concentration an analytical expression for inversion layer capacitance is established.

The variations of electron concentrations in the two

subbands, the average separation of carriers and the eigen energies with the applied field and surface potential are studied. Lastly, the classical and the quantum mechanical inversion layer capacitances are compared. The difference between the classical and the quantum mechanical calculations increases markedly with the applied voltage.

4.2 Suggestions for future work

The mathematical model developed in this work uses only the lower two energy subbands of the inversion layer. In future, a similar model can be developed considering three or more energy subbands for more accurate results. Also the frequency response of the quantum capacitance can be studied using the model developed in this work. Since the quantum mechanical calculation is very time consuming our aim must be to develop a method which can derive a result that approximates the quantum mechanical calculation and that requires the same CPU time as that of the classical calculation. In this thesis we used the triangular well approximation and Airy equation to solve the Schrödinger wave equation. In future similar model can be developed by using variational technique.

REFERENCES

- [1] B.G. Streetman, "Solid state electronic devices," Prentice Hall, New York, 1990, pp. 301-308.
- [2] Yannis P. Tsividis, "Operation and modeling of the MOS transistor," Mc-Graw-Hill Book Company, New York, 1987, pp.47-66.
- [3] F. Stern, "Self-consistent results for n-type Si inversion layers," Physical Review B, Vol.5, No.12, 1972, pp.4891-4899.
- [4] Y. Ohkura, "Quantum effects in Si n-MOS inversion layer at high substrate concentration," Solid State Electronics, Vol.12, 1990, pp.1581-1585.
- [5] Surge Luryi, "Quantum capacitance devices," Applied Physics Letters 52(6), pp. 501-503, 1988.
- [6] Jan Genoe et al., "Capacitances in Double-Barrier Tunneling Structures," IEEE transactions On Electron Devices, Vol.38, No. 9, September, 1991, pp.2006-2012.
- [7] S. Krishnamurthy et al., "Modeling of inversion layer quantization effects in deep submicron n-channel MOS devices," Technical report, Department of Electrical and Computer Engineering, Microelectronic Research Center, The University of Texas at Austin, 1994.

[8] Milton Abramowitz and Irene A. Stegun, "Hand Book of Mathematical Functions," 1964.

[9] E.S. Yang, "Microelectronic Devices," Mc-Graw-Hill Book Company, New York, 1988, pp. 234-237.

